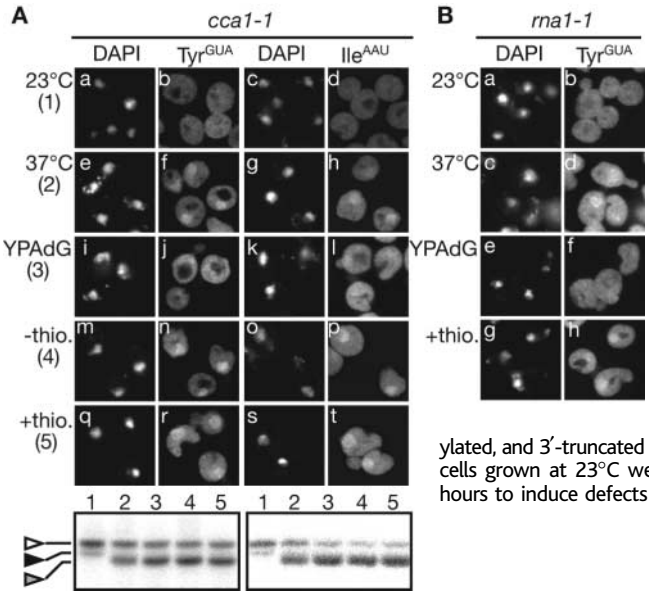

Fig. 4. Various tRNA species are imported into the nucleus, and import is Ran independent. (**A**) *cca1-1* cells grown at 23°C were incubated at 37°C for 3 hours, treated with NaN_3 and 2-dG for 3 hours at 37°C (YPAdG), and then chased without (–thio.) or with (+thio.) thiolutin for 1.5 hours. Samples were analyzed using FISH (top) and Northern hybridization (bottom) with indicated probes. White, black, and gray triangles represent aminoacylated, deacylated, and 3′-truncated tRNAs, respectively. (**B**) *rna1-1* cells grown at 23°C were incubated at 37°C for 1.5 hours to induce defects and then processed as in (A).

the import of both intron-containing and intronless tRNAs requires energy.

We analyzed aminoacylation states of mature tRNAs imported into the nucleus using acidic urea–polyacrylamide gel electrophoresis (urea-PAGE). Mature tRNA-Pro^{UGG} and tRNA-Tyr^{GUA} in Δ*los1* Δ*msn5* cells were present primarily as slower migrating forms even after the chase with thiolutin (Fig. 3C, lanes 1, 3, and 4). These forms were converted to faster migrating forms by base treatment (lane 5), which indicates that the slower migrating tRNAs are aminoacylated. Therefore, imported tRNAs exist mainly in aminoacylated forms in the nucleus.

We asked whether 3′-truncated tRNAs are imported. *cca1-1* cells are deficient in both de novo formation and repair of 3′-terminal CCA ends of tRNAs (*16*), and also in tRNA export (*4*). We therefore treated *cca1-1* cells with NaN_3 and 2-dG at a restrictive temperature to abolish the mature tRNA gradient across the NE and chased them with thiolutin. tRNA-Tyr^{GUA} and tRNA-Ile^{AAU} reaccumulated in the nucleus to similar levels (Fig. 4A, q to t), although the proportions of the 3′-truncated forms of these tRNAs were different (Fig. 4A, bottom). Taken together with the fact that tRNAs in Δ*los1* Δ*msn5* cells were full-length tRNAs, these results indicate that various forms of tRNAs are imported.

To determine the contribution of Ran guanosine triphosphatase (GTPase) (*17*), we examined tRNA import in *rna1-1* cells defective in RanGAP (Ran GTPase activating protein). The *rna1-1* cells accumulated mature tRNA-Tyr^{GUA} in the nucleus at 37°C (*2*), and this tRNA gradient disappeared upon treatment with NaN_3 and 2-dG (Fig. 4B, 37°C, YPAdG). When the cells were transferred to medium with thiolutin, mature tRNA-Tyr^{GUA} was reaccumulated (Fig. 4B, +thio.). Because protein import ceased at 37°C in *rna1-1* cells (fig. S5), these results suggest that tRNA import is Ran independent.

Our results indicate that nuclear mature tRNAs are supplied from the cytosol and that tRNAs shuttle between these two compartments. Shuttling may contribute to tRNA quality control, because tRNAs have long lifetimes and may run the risk of inappropriate modifications (*18*). A quality-control system in the nucleus may repair or filter out inactive tRNAs from those shuttling through the nucleus and provide only active tRNAs back to the cytosol. Another controversial possibility would be to supply tRNAs for nuclear translation (*19*).

References and Notes

1. A. K. Hopper, E. M. Phizicky, *Genes Dev.* **17**, 162 (2003).
2. S. Sarkar, A. K. Hopper, *Mol. Biol. Cell* **9**, 3041 (1998).
3. H. Grosshans, E. Hurt, G. Simos, *Genes Dev.* **14**, 830 (2000).
4. W. Feng, A. K. Hopper, *Proc. Natl. Acad. Sci. U.S.A.* **99**, 5412 (2002).
5. S. Sarkar, A. K. Azad, A. K. Hopper, *Proc. Natl. Acad. Sci. U.S.A.* **96**, 14366 (1999).
6. E. Lund, J. E. Dahlberg, *Science* **282**, 2082 (1998).
7. T. Yoshihisa, K. Yunoki-Esaki, C. Ohshima, N. Tanaka, T. Endo, *Mol. Biol. Cell* **14**, 3266 (2003).
8. R. Azpiroz, R. A. Butow, *Mol. Biol. Cell* **4**, 21 (1993).
9. I. Willis *et al.*, *EMBO J.* **3**, 1573 (1984).
10. K. Hellmuth *et al.*, *Mol. Cell. Biol.* **18**, 6374 (1998).
11. G.-J. Arts, S. Kuersten, P. Romby, B. Ehresmann, I. W. Mattaj, *EMBO J.* **17**, 7430 (1998).
12. A. Kaffman, N. M. Rank, E. M. O'Neill, L. S. Huang, E. K. O'Shea, *Nature* **396**, 482 (1998).
13. M. T. Bohnsack *et al.*, *EMBO J.* **21**, 6205 (2002).
14. E. Lund, S. Güttinger, A. Calado, J. E. Dahlberg, U. Kutay, *Science* **303**, 95 (2004).
15. T. Kadowaki *et al.*, *J. Cell Biol.* **126**, 649 (1994).
16. C. L. Wolfe, A. K. Hopper, N. C. Martin, *J. Biol. Chem.* **271**, 4679 (1996).
17. D. Görlich, U. Kutay, *Annu. Rev. Cell Dev. Biol.* **15**, 607 (1999).
18. S. Kadaba *et al.*, *Genes Dev.* **18**, 1227 (2004).
19. F. J. Iborra, D. A. Jackson, P. R. Cook, *Science* **293**, 1139 (2001).
20. We thank A. K. Hopper, K. Weis, P. A. Silver, Y. Ohya, and J. L. Brodsky for experimental materials and critical reading of our manuscript. We appreciate support from our lab members, especially T. Makio and S. Nishikawa. This work was supported by grants-in-aid for Scientific Research from the Ministry of Education, Culture, Sports, Science, and Technology of Japan.

Supporting Online Material
www.sciencemag.org/cgi/content/full/1113346/DC1
Materials and Methods
SOM Text
Figs. S1 to S6
Tables S1 to S3
References

8 April 2005; accepted 9 May 2005
Published online 19 May 2005;
10.1126/science.1113346
Include this information when citing this paper.

Variable Control of Ets-1 DNA Binding by Multiple Phosphates in an Unstructured Region

Miles A. Pufall,[1] Gregory M. Lee,[2] Mary L. Nelson,[1] Hyun-Seo Kang,[2] Algirdas Velyvis,[3] Lewis E. Kay,[3] Lawrence P. McIntosh,[2] Barbara J. Graves[1]*

Cell signaling that culminates in posttranslational modifications directs protein activity. Here we report how multiple Ca^{2+}-dependent phosphorylation sites within the transcription activator Ets-1 act additively to produce graded DNA binding affinity. Nuclear magnetic resonance spectroscopic analyses show that phosphorylation shifts Ets-1 from a dynamic conformation poised to bind DNA to a well-folded inhibited state. These phosphates lie in an unstructured flexible region that functions as the allosteric effector of autoinhibition. Variable phosphorylation thus serves as a "rheostat" for cell signaling to fine-tune transcription at the level of DNA binding.

Proteins are activated or repressed by posttranslational modifications in response to extracellular cues. Phosphorylation, a typical modification, often accumulates at multiple sites until a threshold level is reached. The outcome is described as a sharp on/off switch of protein activity (*1*, *2*). However, biological processes may need more sensitive regulation. Despite this need, variable regulation of protein activity in response to multiple modifica-

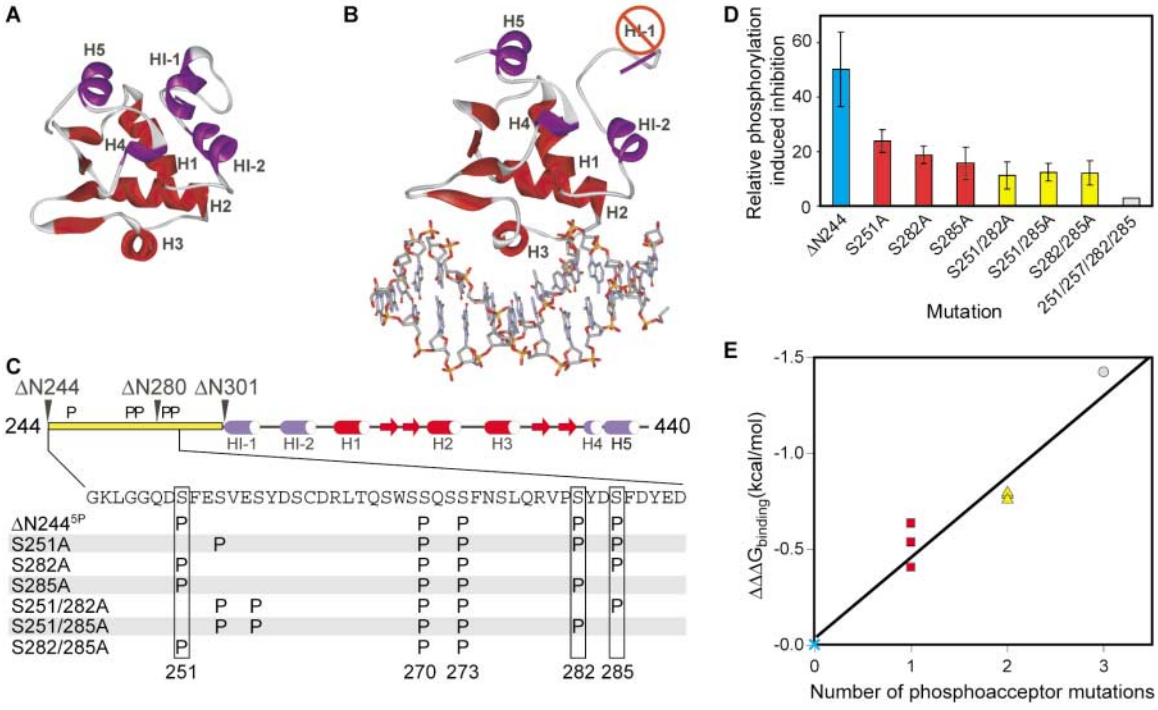

Fig. 1. Differential phosphorylation of Ets-1 leads to variable DNA binding affinity. (**A**) NMR-derived structure of the partially active Ets-1 truncation ΔN301, showing the ETS domain (red) and inhibitory helices (purple) (*8*). (**B**) Crystallographic structure of DNA-bound ΔN280, showing inhibitory helix HI-1 unfolded (*31*). (**C**) Schematic secondary structure of ΔN244 with SRR (yellow) and sites phosphorylated by CaMKII in vitro (labeled P) as determined by mass spectrometry and/or NMR for the wild type and mutants. Boxed phosphoserines are critical for the reinforcement of autoinhibition. Additional phosphates have negligible individual effects and vary with mutation pattern (*32*). (**D**) Relative phosphorylation-induced inhibition = $K_{D(\text{phosphorylated mutant})}/K_{D(\text{unmodified mutant})}$ with the standard error of the ratio ($n \geq 4$ replicas) (*15*). Single mutants are colored red and double mutants are colored yellow. The quadruple mutant (gray) (*11*) provides expected data for the disruption of three critical phosphoacceptor sites (251, 282, and 285). (**E**) $\Delta\Delta G^{\circ}_{binding} = -RT$ ln(relative induced inhibition, ΔN244) + RT ln(relative induced inhibition, mutant), where R is the ideal gas constant and T is temperature, is plotted as a function of the number of phosphoacceptor mutations (wild type, exes; single, squares; double, triangles; triple, circle). The linear relationship (correlation coefficient $r = 0.96$) implicates additivity of mutational effects (*33*).

tions has not been documented. Here we show how the transcription factor Ets-1 exhibits graded DNA binding activity with different levels of phosphorylation.

Ets-1 is regulated by an autoinhibitory module composed of four α helices (HI-1, HI-2, H4, and H5) that flank the DNA-binding ETS domain. In the native protein, these helices pack cooperatively on a surface of the ETS domain that is opposite to the DNA binding interface (Fig. 1A), reducing the affinity of Ets-1 for DNA 10-fold, compared with the affinity of the minimal ETS domain (*3*–*5*). This inhibitory module opposes the structural change that accompanies DNA binding, the most striking feature of which is the unfolding of inhibitory helix HI-1 (Fig. 1B) (*3*, *6*–*8*). Recent nuclear magnetic resonance (NMR) spectroscopic studies indicate that helix HI-1 is labile, even in the absence of DNA, and could serve as a control point for modulating DNA binding affinity (*8*). Cooperative DNA binding with runt-related protein 1 (RUNX1) counteracts autoinhibition, activating the binding of native Ets-1 ~10-fold (*9*), whereas Ca^{2+}-dependent phosphorylation of Ets-1 at multiple sites reinforces autoinhibition by lowering DNA affinity ~50-fold further to an overall inhibition of 500- to 1000-fold (fig. S1, A to D) (*10*, *11*). The modulation of Ets-1 DNA binding is correlated with transcriptional activity in in vivo assays and is responsive to cellular cues (*12*–*14*). For example, Ca^{2+} signaling in vivo disrupts Ets-1 DNA binding and reduces the transcription of Ets-1–driven reporters (*13*). We show that this multiple phosphorylation is not simply an on/off switch, but rather an incremental rheostat-like control for Ets-1 binding activity.

We used a minimal fragment, ΔN244, which displays the DNA binding properties of full-length Ets-1 (fig. S1, A to D) (*11*, *15*). $\Delta N244^{5P}$, a form which is homogenously phosphorylated by CaMKII, contains five specific phosphoserines in the serine-rich region (SRR, residues 244 to 300) (Fig. 1C) and appears to undergo the same structural transition upon DNA binding as do unmodified ΔN244 (fig. S1E) and other Ets-1 species (*3*, *7*, *11*).

In cells, Ets-1 is variably phosphorylated in response to Ca^{2+} release (*10*). To gauge the effect of differential phosphorylation on activity, we mimicked in vivo phosphorylation by mutating phosphoacceptor serines to alanines singly and in pairs (Fig. 1C), and we then measured the DNA binding affinity of phosphorylated and unmodified forms. Mutation of three (251, 282, and 285) of the five serines, but not two others (270 and 273), significantly reduced inhibition. Furthermore, mutation of one, two, or all three critical sites (*11*) yielded a graded reduction in phosphorylation-dependent inhibition (Fig. 1D), with each phosphate contributing additively to the change in the free energy of binding (Fig. 1E). This finding shows that the number and context of sites, and not simply a buildup of charge, affects inhibition. Thus, in contrast to proteins such as Sic1 (*2*) and NFAT1 (nuclear factor of activated T cells) (*1*, *16*), for which a threshold level of phosphorylation serves as a binary switch, multiple sites within Ets-1 regulate DNA binding in a graded manner across a wide range of affinities, which is consistent with observed variable regulation in vivo (*13*).

The phosphorylated SRR was found to be predominantly unstructured and highly flexible. Based on main-chain ^{1}H and ^{13}C chemical shifts, NMR spectra revealed no predominant secondary structure within this region (*17*) (Fig. 2A), and the amide hydrogen exchange (HX) rates were comparable to those of a random coil polypeptide (Fig. 2B). Further, NMR relaxation experiments demonstrated a high degree of backbone conformational mobility on nanosecond to picosecond time scales (Fig. 2C). Thus, the dynamic phosphorylated SRR may impart variable regulation of DNA binding by making

[1]Huntsman Cancer Institute, Department of Oncological Sciences, University of Utah, Salt Lake City, UT 84112–5550, USA. [2]Department of Biochemistry and Molecular Biology, Department of Chemistry, and The Michael Smith Laboratory, University of British Columbia, Vancouver, British Columbia, V6T 1Z3, Canada. [3]Departments of Medical Genetics, Biochemistry, and Chemistry, University of Toronto, Toronto, Ontario, M5S 1A8, Canada.

*To whom correspondence should be addressed. E-mail: Barbara.Graves@hci.utah.edu

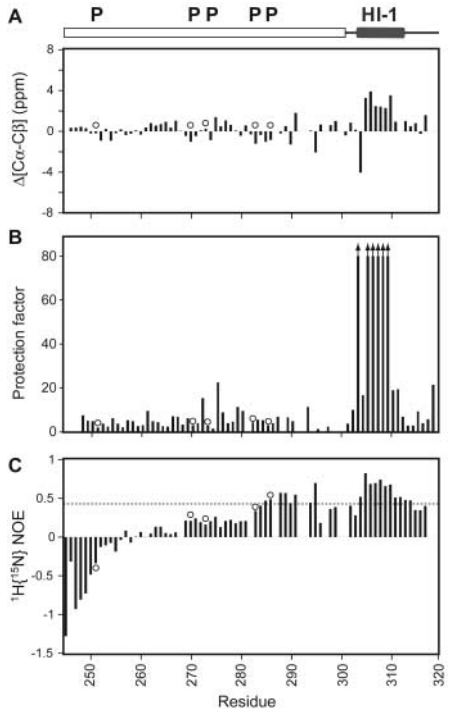

Fig. 2. The phosphorylated SRR is predominantly unstructured and flexible. Panels present data for residues 244 to 320 of ΔN244^{5P} (*15*). Circles and P denote the five phosphoserines. Missing data correspond to prolines, or residues with spectral overlap and/or weak signals. (**A**) In contrast to HI-1, differences between the observed and random coil ($^{13}C^{\alpha}$-$^{13}C^{\beta}$) chemical shifts indicated an absence of any detectable secondary structure in the SRR (*17*). (**B**) Small protection factors (k_{pred}/k_{ex}) demonstrate that backbone SRR amides undergo HX at rates (k_{ex}) similar to those predicted for a random coil polypeptide (k_{pred}). Amides within HI-1 do not show measurable HX by the CLEANEX method ($k_{ex} < 0.5\ s^{-1}$, protection factors > 80). (**C**) Small or negative heteronuclear $^{1}H\{^{15}N\}$ nuclear Overhauser enhancement values indicate a high degree of flexibility. The horizontal line at 0.4 marks an approximate boundary between flexible (below) and rigid (above) amides on a subnanosecond time scale (*34*).

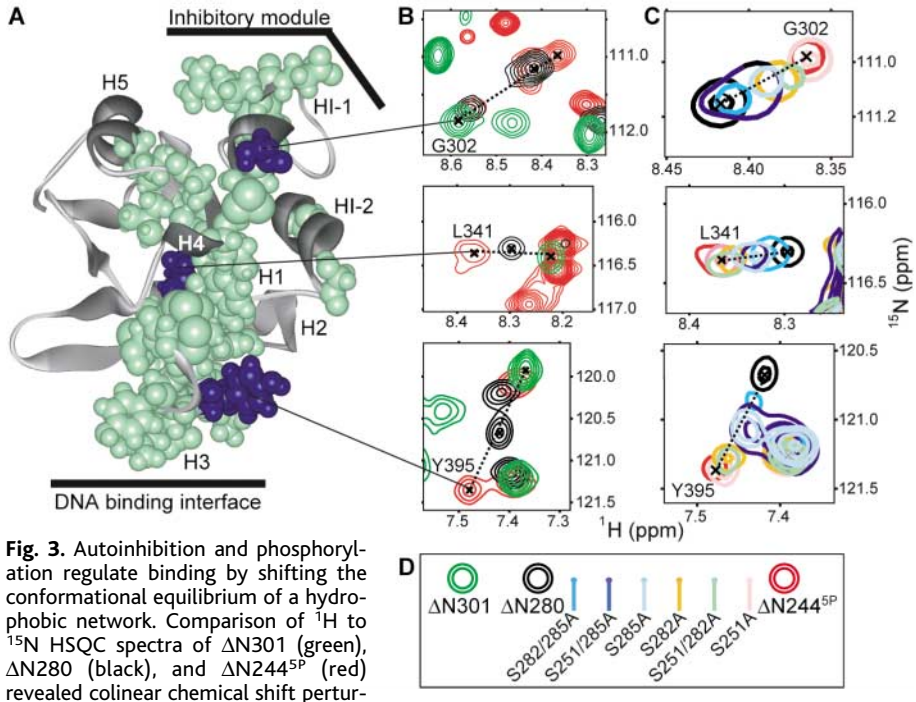

Fig. 3. Autoinhibition and phosphorylation regulate binding by shifting the conformational equilibrium of a hydrophobic network. Comparison of ^{1}H to ^{15}N HSQC spectra of ΔN301 (green), ΔN280 (black), and ΔN244^{5P} (red) revealed colinear chemical shift perturbations among ~25 common residues in the three species (table S1 and fig. S3) (*15*). (**A**) Shifted residues depicted on the NMR-derived structure of ΔN301 by van der Waals surfaces (*8*). (**B**) Spectral overlays highlight the progressive shift changes (black exes and dashed lines) for G302, L341, and Y395 (*20*). (**C**) Peaks from six phosphorylated phosphoacceptor mutants follow the same colinear chemical shift pattern (between ΔN280 and ΔN244^{5P} peaks on dashed lines). (**D**) Color key and consensus relative peak positions.

transient interactions with the remainder of the protein.

Despite this flexibility, the SRR has a profound impact on the structure, stability, and dynamics of the DNA binding domain and on the inhibitory helices. We compared three Ets-1 fragments with increasing levels of inhibition: partially activated ΔN301; ΔN280, a minimal fragment that recapitulates unmodified autoinhibited Ets-1 binding; and ΔN244^{5P} (dissociation constants $K_D \sim 10^{-11}$, 10^{-10}, and 10^{-8} M, respectively) (fig. S1, A, B, and D) (*6*, *8*, *18*). The comparison of ^{1}H-^{15}N heteronuclear single quantum correlation (HSQC) spectra detected significant changes in backbone amide chemical shifts for ~25 residues common to the three species, indicative of structural perturbations (figs. S2 and S3 and table S1). The labile inhibitory helix HI-1 and helices H1 and H3 of the DNA binding domain were most widely affected. The perturbed residues, many of which are nonpolar, form a hydrophobic network connecting the inhibitory elements and the DNA binding interface (Fig. 3A). Mutation of leucine-429 to alanine within this network reduced autoinhibition and impaired phosphorylation reinforcement (fig. S1C) (*5*, *11*), indicating that the integrity of this hydrophobic network is required for regulation.

A striking linear pattern of change was observed from ΔN301 to ΔN280 to ΔN244^{5P} in the amide ^{1}H and ^{15}N chemical shifts of almost all of the affected residues (Fig. 3B and table S1). This progressive colinear pattern is a signature of an allosterically regulated molecule that is in conformational equilibrium between at least two states, with the intermediate chemical shifts representing a population-weighted average of these states (*19*). Based on the correlation between the linear pattern of amide chemical shifts with DNA binding affinity (*20*), we propose that free Ets-1 exists in equilibrium between an active state (represented most closely by ΔN301), which is poised to bind DNA, and an inactive state (represented by ΔN244^{5P}). According to this allosteric model, Ets-1 DNA binding affinity reflects the balance of these two states.

A comparison of the backbone amide chemical shifts of phosphorylated ΔN244 with single or double serine-to-alanine mutations also revealed a colinear shifting pattern between ΔN280 and ΔN244^{5P} in at least 16 of the 25 residues within the aforementioned hydrophobic network. The position of the chemical shifts for each species, phosphorylated at the remaining CaMKII sites, roughly correlated with affinity. This finding emphasizes the context dependence of each phosphate and suggests that each has a distinct role in modulating the conformational equilibrium (Fig. 3, C and D, and table S1). These NMR studies show that differential phosphorylation regulates DNA binding by fine-tuning the balance between the active and inactive states of Ets-1.

Amide HX experiments helped characterize the dynamics of the active and inactive states (Fig. 4, A to C, and fig. S4). Consistent with previous studies (*8*), backbone amides within the inhibitory helices HI-1 and HI-2, as well as the DNA binding helix H3 of the active ΔN301, exhibited limited protection from exchange, indicating that these helices sample locally unfolded conformations even in the absence of DNA. In contrast, the same amides exhibited elevated HX protection within ΔN280, and further in ΔN244^{5P}, suggestive of a progressively less dynamic and more stably folded species. The dynamic active state and more stable inactive state are consistent with previous studies, showing that affinity for DNA decreases as the propensity of helix HI-1 to unfold decreases (*3*, *7*, *11*).

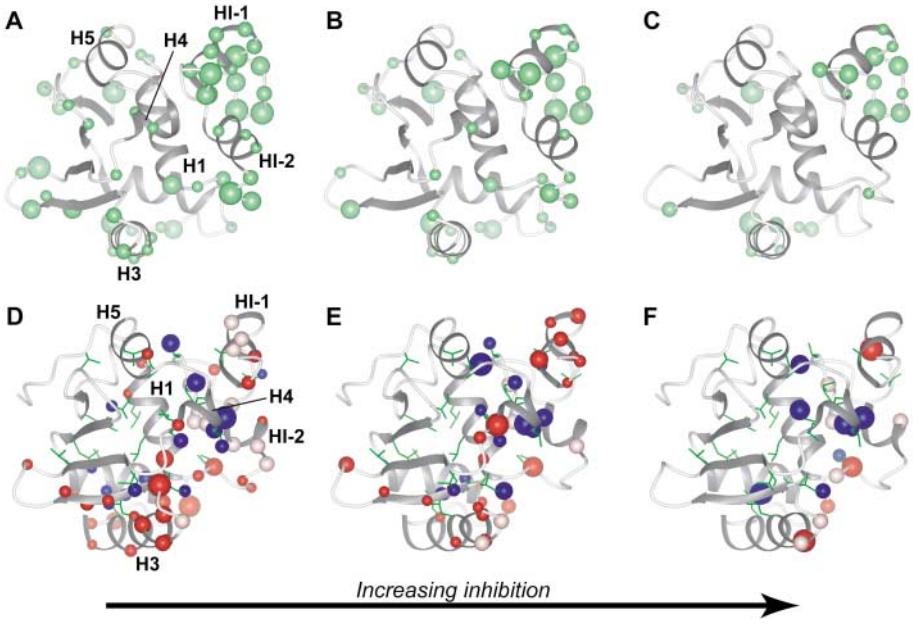

Fig. 4. Concerted motion of the hydrophobic network is dampened by autoinhibition and phosphorylation. ΔN301 (**A** and **D**), ΔN280 (**B** and **E**), and ΔN244^{5P} (**C** and **F**) were analyzed by amide HX and backbone and side-chain relaxation dispersion (*15*). Relative values (figs. S4 to S6) are highlighted on the NMR-derived structure of ΔN301 (*8*). [(A), (B), and (C)] For backbone HX, amides exhibiting measurable exchange (k_{ex} > 0.5 s^{-1}) are depicted by green balls with diameters scaled according to increasing k_{ex}. [(D), (E), and (F)] For relaxation dispersion, backbone and Trp side-chain nitrogens (red balls) and ^{13}C methyls of Ile$^{\delta1}$, Val, and Leu (blue balls) with $R_{ex} \geq 2$ s^{-1} are shown, where the diameter of the balls increases in proportion to R_{ex} at 800 MHz (the largest balls correspond to $R_{ex} \geq 15$ s^{-1}). Pink balls represent atoms whose NMR signals are broadened beyond detection. Ile, Leu, and Val side chains are shown as green sticks.

A dynamic connection between the autoinhibitory module and the DNA binding interface was demonstrated by NMR backbone amide and side-chain methyl relaxation dispersion measurements (Fig. 4, D to F, and figs. S5 and S6) (*21*). The contribution of millisecond to microsecond time scale motions to linewidth broadening, denoted R_{ex}, is indicative of conformational switching. Consistent with previous studies (*8*), the backbone amides of ΔN301 exhibited mobility on this time scale (exchange lifetimes $\tau_{ex} \sim$ 0.3 ms) for residues that shift colinearly between ΔN301, ΔN280, and ΔN244^{5P}. These motions were dampened in ΔN280, and further in ΔN244^{5P} (Fig. 4, red balls). ^{13}C methyl relaxation dispersion of Leu, Ile, and Val side chains within the hydrophobic network of ΔN301 showed motions on the same time scale ($\tau_{ex} \sim$ 0.3 ms) that again were progressively reduced in ΔN280 and ΔN244^{5P} (Fig. 4, blue balls). These data indicate that the core hydrophobic packing of Ets-1 is dynamic in the active state and that increasing inhibition attenuates these motions. Localized collective motions on a similar time scale within both the backbone and side chains support our proposal that the inhibitory module, DNA binding interface, and hydrophobic core form a concerted unit that is linked as a dynamic hydrophobic network. Furthermore, the HX and R_{ex} data are consistent with a conformational equilibrium within this concerted unit between at least two states: one stable and inactive, another more dynamic and active.

The dynamic character of Ets-1 is likely essential for sequence-specific DNA binding but also provides an opportunity for regulation (*22*, *23*). NMR studies of the *Escherichia coli* lactose repressor protein suggest that fluctuations on a millisecond to microsecond time scale are necessary for facilitated diffusion on nonspecific DNA, as well as facile adoption of a specifically bound conformation (*24*). The active state of Ets-1 is similarly poised to adopt a high-affinity interaction with DNA. In this case, signal-dependent phosphorylation employs these motions to vary activity in a graded manner.

The surprising use of a highly flexible segment in the graded regulation of Ets-1 DNA binding adds to the growing recognition of the role of unstructured protein regions in biology (*25*). These flexible elements often display posttranslational modifications [for example, MAPK Ets-1 phosphorylation (*26*), histone tails (*27*), and SH2 domain targets (*28*)], tether independent domains [for example, protein kinase A (PKA) (*29*)], or require folding for activity [for example, the cyclic adenosine 3′,5′-monophosphate response element binding protein (CREB) and the CREB binding protein (*30*)]. The highly mobile SRR demonstrates a role for unstructured protein segments in integrating signals that direct the variable regulation of protein activity.

References and Notes

1. C. Salazar, T. Höfer, *J. Mol. Biol.* **327**, 31 (2003).
2. S. Orlicky, X. Tang, A. Willems, M. Tyers, F. Sicheri, *Cell* **112**, 243 (2003).
3. J. M. Petersen *et al.*, *Science* **269**, 1866 (1995).
4. M. D. Jonsen, J. M. Petersen, Q. Xu, B. J. Graves, *Mol. Cell. Biol.* **16**, 2065 (1996).
5. H. Wang, L. P. McIntosh, B. J. Graves, *J. Biol. Chem.* **277**, 2225 (2002).
6. J. J. Skalicky, L. W. Donaldson, J. M. Petersen, B. J. Graves, L. P. McIntosh, *Prot. Science* **5**, 296 (1996).
7. C. W. Garvie, M. A. Pufall, B. J. Graves, C. Wolberger, *J. Biol. Chem.* **277**, 45529 (2002).
8. G. M. Lee *et al.*, *J. Biol. Chem.* **280**, 7088 (2005).
9. T. L. Goetz, T. L. Gu, N. A. Speck, B. J. Graves, *Mol. Cell. Biol.* **20**, 81 (2000).
10. B. Rabault, J. Ghysdael, *J. Biol. Chem.* **269**, 28143 (1994).
11. D. O. Cowley, B. J. Graves, *Genes Dev.* **14**, 366 (2000).
12. D. Baillat, A. Bègue, D. Stéhelin, M. Aumercier, *J. Biol. Chem.* **277**, 29386 (2002).
13. H. Liu, T. Grundström, *Mol. Biol. Cell* **13**, 4497 (2002).
14. W. Sun, B. J. Graves, N. A. Speck, *J. Virol.* **69**, 4941 (1995).
15. Materials and methods are available as supporting material on *Science* Online.
16. H. Okamura *et al.*, *Mol. Cell* **6**, 539 (2000).
17. D. S. Wishart, B. D. Sykes, *J. Biomol. NMR* **4**, 171 (1994).
18. Limited solubility of ΔN244 prevented assignment of resonances within the molecule. However, the HSQC spectra of ΔN244 and ΔN280 were essentially superimposable.
19. B. F. Volkman, D. Lipson, D. E. Wemmer, D. Kern, *Science* **291**, 2429 (2001).
20. The series does not adhere strictly to a two-state model because the position of ΔN280 does not scale consistently with activity at every residue. Nevertheless, the mean relative change in chemical shift [$|\delta(\Delta N301 - \Delta N280)|$]/[$|\delta(\Delta N301 - \Delta N244^{5P})|$] is 67 ± 16% for 25 residues, consistent with 80% estimated from affinity (*15*).
21. F. A. Mulder, A. Mittermaier, B. Hon, F. W. Dahlquist, L. E. Kay, *Nat. Struct. Biol.* **8**, 932 (2001).
22. V. A. Feher, J. Cavanagh, *Nature* **400**, 289 (1999).
23. D. Kern, E. R. Zuiderweg, *Curr. Opin. Struct. Biol.* **13**, 748 (2003).
24. C. G. Kalodimos *et al.*, *Science* **305**, 386 (2004).
25. P. E. Wright, H. J. Dyson, *J. Mol. Biol.* **293**, 321 (1999).
26. C. M. Slupsky *et al.*, *Proc. Natl. Acad. Sci. U.S.A.* **95**, 12129 (1998).
27. B. P. Hudson, M. A. Martinez-Yamout, H. J. Dyson, P. E. Wright, *J. Mol. Biol.* **304**, 355 (2000).
28. P. J. Finerty Jr., A. K. Mittermaier, R. Muhandiram, L. E. Kay, J. D. Forman-Kay, *Biochemistry* **44**, 694 (2005).
29. C. Kim, N. H. Xuong, S. S. Taylor, *Science* **307**, 690 (2005).
30. I. Radhakrishnan *et al.*, *Cell* **91**, 741 (1997).
31. C. W. Garvie, J. Hagman, C. Wolberger, *Mol. Cell* **8**, 1267 (2001).
32. Single-letter abbreviations for the amino acid residues are as follows: A, Ala; C, Cys; D, Asp; E, Glu; F, Phe; G, Gly; H, His; I, Ile; K, Lys; L, Leu; M, Met; N, Asn; P, Pro; Q, Gln; R, Arg; S, Ser; T, Thr; V, Val; W, Trp; and Y, Tyr.
33. J. A. Wells, *Biochemistry* **29**, 8509 (1990).
34. L. E. Kay, D. A. Torchia, A. Bax, *Biochemistry* **28**, 8972 (1989).

35. We acknowledge support from NIH grant R01 GM38663 (B.J.G.); NIH grants T32-CA93247 and -GM08537 (M.A.P.); P01-CA24014 (Huntsman Cancer Institute) and the U.S. Department of Energy and the Huntsman Cancer Foundation (B.J.G.); the National Cancer Institute of Canada with funds from the Canadian Cancer Society (L.P.M.); the Government of Canada's Network of Centres of Excellence Program supported by the Canadian Institutes of Health Research (CIHR); the Natural Sciences and Engineering Research Council through the Protein Engineering Network of Centres of Excellence (L.P.M. and L.E.K.); and the CIHR for a Scientist Award (L.P.M.) and funding (L.E.K.). L.E.K. holds a Canada Research Chair in Biochemistry.

Supporting Online Material

www.sciencemag.org/cgi/content/full/309/5731/142/DC1
Materials and Methods
Figs. S1 to S6
Table S1
References

7 March 2005; accepted 11 May 2005
10.1126/science.1111915